Study of Base Isolation Systems

by

Saruar Manarbek

Bachelor of Engineering in Civil Engineering
University of Warwick, 2012

Submitted to the Department of Civil and Environmental Engineering
in Partial Fulfillment of the Requirements for the Degree of

Master of Engineering
at the

Massachusetts Institute of Technology

June 2013

Signature of Author:

Department of Civil and Environmental Engineering
May 21, 2013

Certified by:

Jerome J. Connor
Professor of Civil and Environmental Engineering
Thesis Supervisor

Accepted by:

Heidi Nepf
Chair, Departmental Committee for Graduate Students

Study of Base Isolation Systems

by

Saruar Manarbek

Submitted to the Department of Civil and Environmental Engineering
in May, 2013 in Partial Fulfillment of the Requirements
for the Degree of Master of Engineering in Civil and Environmental Engineering

Abstract

The primary objective of this investigation is to outline the relevant issues concerning the conceptual design of base isolated structures. A 90 feet high, 6 stories tall, moment steel frame structure with tension cross bracing is used to compare the response of both fixed base and base isolated schemes to severe earthquake excitations. Techniques for modeling the superstructure and the isolation system are also described.

Elastic time-history analyses were carried out using comprehensive finite element structural analysis software package SAP200. Time history analysis was conducted for the 1940 El Centro earthquake. Response spectrum analysis was employed to investigate the effects of earthquake loading on the structure. In addition, the building lateral system was designed using the matrix stiffness calibration method and modal analysis was employed to compare the intended period of the structure with the results from computer simulations. Base isolation proves to be effective in reducing the induced inertia forces on a structure by increasing the effective period of oscillation.

Keywords: Base Isolation, time history analysis, response spectrum analysis, matrix stiffness calibration method.

Thesis supervisor: Jerome J. Connor
Title: Professor of Civil and Environmental Engineering

Acknowledgments

First and foremost, I would like to extend my deep gratitude to my family, without whom my education would not be possible. To my family, who inspired and encouraged me to go my own way, I am forever thankful for their unconditional love and support. I am further thankful for my parents' hard work which enabled them to give me the opportunity to obtain the kind of education I dreamed about.

I am particularly grateful for the assistance given by Professor Jerome Connor for his patient guidance, enthusiastic encouragement and useful critiques of this work. I would also like to thank Dr. Pierre Ghisbain, for his advice and assistance. His willingness to give his time so generously has been very much appreciated.

Lastly, many members of the MIT community contributed to my well-being here. Thank you, fellow students of the MEng class of 2012-2013 for your advice, support and company. I am very glad I had a chance to spend a year studying together with extraordinary individuals like you.

Table of Contents

List of Figures

Chapter 1

Introduction

The aim of this work is to design a base isolation system for a low rise building and to evaluate its performance using various techniques including dynamic time history analysis, static pushover analysis. Characteristics of base isolation devices currently available on the market will be evaluated and compared. The main comparison criteria are cost, durability, residual displacement and ability to provide wind resistance.

1.1 General Overview

A traditional "brute force" method for making earthquake resistant structures is to design a stiff and strong enough structure so that it could accommodate foreseeable lateral forces. This may not be the most cost efficient method. The problem with this method is that the building has to absorb all the lateral forces induced by the seismic ground motion. The technique of base isolation allows to go around the aforementioned problem.

The method of base isolation was developed in an attempt to mitigate the effects of earthquakes on buildings during earthquake attacks and has been practically proven to be one of the very effective methods in the past several decades. Base isolation consists of the installation of the support mechanisms, which decouple the structure from earthquake induced ground motions. Base isolation allows to filter the input forcing function and to avoid the acceleration induced seismic forces on the structure. If the structure is separated from the ground during an earthquake, the ground is moving but the structure experiences little movement. This technology was first introduced in the 1900's but it only evolved into the practical strategy for seismic design in the

1970's.

The fundamental goal of base isolation is to reduce substantially the absorption of the earthquake induced forces and energy by the structure. This is accomplished by placing a structure on a support mechanism with low lateral stiffness so that in the event of an earthquake, when the ground undergoes strong motion, only moderate motion is induced in the structure itself. As the flexibility of the support bearings increases (stiffness decreases), movement of the structure relative to the ground under wind loads may become a problem. It has been indicated that a base isolator with hysteric force-displacement characteristics provides the required high flexibility, high damping and force limitation under earthquake loads, while at the same time sufficiently high stiffness under smaller loads to handle wind induced horizontal forces [Skinner and McVerry, 1975].

Connor [2002] gave an introduction to the fundamentals in analyzing the response of base isolation mechanisms through a two degree of freedom linear dynamic system. Base isolation mitigates seismic response through shifting the effective fundamental frequency of the system out of the range where earthquake would produce greatest inertia forces. Increased flexibility of support bearings (or their decreased stiffness) increases the equivalent natural period of the system. Because period is increased beyond the period range of the earthquake induced ground motion, resonance is avoided and the seismic acceleration response is reduced.

The success of a base isolation system in a building depends on the parameters of bearing mechanisms, which decouple the structure from the ground motions. Therefore, it is of extreme importance to have an understanding of the influence of parameters of the support systems and the structure on the seismic performance base isolated structures. Low stiffness of the support mechanisms in a base isolated structure gives a building a long effective period and therefore reduces the earthquake generated lateral inertia forces on the structure. Numerous types of base isolation devices have been developed to accomplish this function, such as laminated elastometric rubber bearings, lead rubber bearings, yielding steel devices, friction devices (PTFE sliding bearings) and lead extrusion devices.

Andriono [1990] suggested that base isolation systems significantly reduce the superstructure lateral stiffness and ductility demands compared to unisolated structures. This allows cost savings from less materials being spent on lateral systems and simplification of structural detailing. In addition, base isolation enables a wider range of architectural forms and structural materials to be available to the designer.

Beside the technical feasibility, a key parameter that needs to be approached in the early phases of design is economic feasibility. The principal factors to be evaluated

are construction costs, earthquake insurance premiums, damage costs in case of an earthquake, maintenance costs, loss of market share and potential liability [Charng, 1998]. Skinner and McVerry [1975] indicated that the current base isolation practices may often result in significant reductions in the cost of providing the necessary level of seismic resistance to buildings.

In the past several decades the technique of base isolation has been increasingly accepted for providing seismic protection to structures and their contents. Base isolation as a technique for the seismic retrofit of historic structures, designing buildings containing motion sensitive equipment (such as computer systems facilities), high risk buildings (such as nuclear power plants), buildings of special importance after earthquakes (hospitals, disaster management centers) etc.

Therefore, under the aforementioned circumstances, base isolation does indeed have advantages over traditional approaches by providing much higher protection from extreme earthquake events. Base isolations systems are believed to provide solutions for a wide range of design situations.

1.2 Earthquake Induced Motion

In order to understand the motion of buildings it is necessary to identify the applied forces. This section will outline major fundamental issues associated with earthquakes.

1.2.1 Earthquake Characteristics

An engineer must understand the meaning of the main characteristics of earthquake ground motion, which are:

- duration
- displacement amplitude
- velocity amplitude
- acceleration amplitude
- ground motion frequency content (or frequency range)

Buildings also have a set of natural frequencies that characterize their response. The lowest frequency is called fundamental frequency (or frequency of the first mode). As the induced earthquake frequency approaches the fundamental frequency resonance

occurs. A designer has to ensure that the fundamental building frequency is beyond frequency content is beyond the frequency range of an earthquake. A rule of thumb that is quite useful in the preliminary design gives an approximate relation of the fundamental period T, to the number of stories n, in a building.

$$T = \frac{n}{10} \tag{1.1}$$

Therefore, a 90 feet tall meter building with a story height of 15 feet would have 6 stories and its period can be approximated to around 0.6 seconds.

1.2.2 Resonance Phenomenon

As mentioned before, engineers must design buildings so that the frequency range of the building's response to ground motion was away from the frequency content of earthquakes. If the building's response frequency is coincident or close to the frequency of ground motion, resonance occurs. Resonance may be catastrophic as it amplifies the building response, hence the lateral inertia forces on a building are amplified. A famous example of a catastrophic failure due to resonance is the Tacoma Narrows bridge. However, failure of the Tacoma Narrows bridge was not caused by ground motion, but rather by wind induced oscillatory vortex shedding, whose frequency coincided with one of the torsional vibration modes of the bridge about the longitudinal axis of the deck. Wind induced resonance is beyond the scope of this work; nevertheless, the case of the Tacoma Narrows bridge is an excellent example of catastrophic structural failures caused by resonance.

Figure 1.1 – Tacoma Narrows Bridge: excessive deformation and subsequent collapse due to resonance

1.2.3 Response Spectra

A response spectrum succinctly represents the building's range of responses to ground motion for a range of frequencies. The building response spectrum is commonly represented as a graph which plots the the maximum response values of acceleration against the period of excitation (inverse of frequency). Engineers first determine the building's fundamental mode frequency, and then, using the aforementioned graph determine the acceleration that a building will undergo in the event of an earthquake. The amount of *structural* damage a structure will experience is proportional to the inter-story drift of the building. Therefore, analyzing the structure to find its response frequencies, is of chief importance when investigating the seismic behavior of a building.

1.3 Building Response

The following section will briefly discuss the main parameters affecting the building response ad earthquake damage. A building may undergo various types of damage from minor cracking in surface finishes to major cracks in the main structural elements, which may lead to total structural failure. Damage is generally divided into two groups: structural (damage to structural components due to displacements) and non-structural (damage to the contents of the building due to accelerations). Structural damage may cause significant loss of life and property. Non-structural damage, although may potentially cause loss of life, is primarily connected with loss of property and possible injuries.

1.3.1 Effects of Ground Acceleration

In order to understand how a structure undergoes damage from ground acceleration, one needs to employ Newton's Second Law of Motion, which states the force acting upon a body equals mass of the body times its acceleration. Consequently, as acceleration increases so do the forces on a building. Therefore, in order to reduce forces on a structure, an engineer must decrease the building acceleration. The product of mass and acceleration is defined as the inertia force. Inertia force due to ground motion causes the structure to deform, inducing deformations beams, columns, lateral braces, bearing walls, connections and other structural members.

1.3.2 Effects of Stiffness and Ductility

Stiffness is dependent on height, materials, connections, lateral systems etc. Stiffness has a great effect on lateral forces on experienced by the structure due to ground motion. An infinitely stiff building will experience accelerations equal to those of the ground. Therefore, lateral inertia forces on a building due to ground motion will be greater, the greater the building stiffness is. Base isolation is a system that effectively reduces the equivalent stiffness of the system, thus reducing the inertia forces on the structure.

In traditional seismic design, the ductility of a structure is the most important factor defining the building's seismic performance. The main task of an engineer designing an earthquake resistant structure is to ensure a building has sufficient ductility to withstand the earthquakes it may experience during its lifetime.

1.3.3 Effects of Damping

Damping is defined as the decay of amplitude of oscillation over time. Every building has some inherent damping. Without damping, an oscillating body would never come to rest. Damping in buildings is due to internal friction which dissipates input energy. The greater the building's intrinsic damping, the better the building will dissipate the input earthquake energy.

Chapter 2

Components of Base Isolation Systems

Since, the concept of seismic base isolation has been in use for the last several decades, the technology is mature and there exists a variety of base isolation devices. The devices can be divided into two major groups: elastometric systems and sliding systems. Both isolations systems have some inherent damping and both are employed to shift the fundamental building frequency beyond the range of earthquake excitation, thus reducing the accelerations and reducing the corresponding lateral inertia forces. The devices of both groups are defined by a particular set of characteristics such as: stiffness and corresponding service load deformations, yield strength and maximum displacements under extreme earthquake loads, residual displacements and the ability to return to initial position (resilience), vertical stiffness etc. This chapter will outline the aforementioned parameters for a number of devices currently available in the market.

2.1 Elastometric Devices

Elastometric devices are characterized by their name as they source their effectiveness from being composed of elastometric material. Their main advantage is their resilience. However service load deformations and durability may be an issue. The common elastometric devices include: natural rubber bearings, lead rubber bearings and high damping natural rubber bearings. The details of the aforementioned devices will be discussed in this section.

2.1.1 Natural Rubber Bearings

Natural rubber bearings, also known as laminated rubber bearings are manufactured of either natural rubber or neoprene, a synthetic rubber material employed of its toughness and durability, which has a behavior similar to natural rubber [Ehrlich et al., 1980]. A typical natural rubber bearing arrangement is shown in Figure 2.1

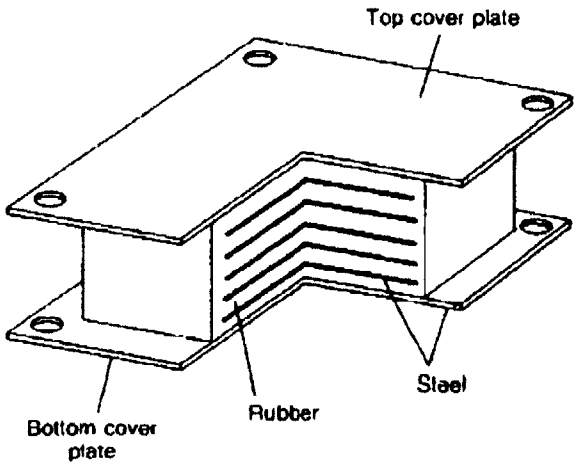

Figure 2.1 – Natural rubber bearing schematic [Kunde and Jangid, 2003]

Natural rubber bearings are comprised of the alternating rubber and steel shim layers. These layers are joined together by means of the vulcanization process under pressure and heat to produce a composite bearing. Steel shims add vertical stiffness to the bearings and hence prevent the rocking response of an isolated structure. In addition steel shims prevent rubber from bulging out under high axial compressive loads. The shims have no effect on lateral stiffness of bearings as it is controlled by the shear modulus of the elastic material. The bearings are mounted between two thick endplates to facilitate the connection between the foundations and the isolation mat.

The primary drawbacks of natural rubber bearings are low damping and inability to handle service wind loads due to low stiffness. Normally natural rubber bearings exhibit 2-3% of critical damping. Damping characteristics can be increased by changing the properties of elastometric material but normally, natural rubber bearing support system requires additional damping devices, such as viscous or hysteretic dampers to deal with service and extreme seismic loads.

However, natural rubber bearings are easy to install and manufacture. Their behavior can also be easily modeled analyzed and hence designed. The effects of creep, stiffness

deterioration over time are small because natural rubber and neoprene are known to have a consistent shear modulus over time [Naeim and Kelly, 1999].

2.1.2 Lead Rubber Bearings

In comparison to natural rubber bearings, lead rubber bearings have a much better capability to provide adequate stiffness for wind loads and better damping characteristics. The lead rubber bearing configuration is the same as that of natural rubber bearings, except there is one or more cylindrical lead plugs in the center as shown in Figure 2.2. The lead plug in combination with the rubber causes the device to demonstrate bilinear behavior. Under low service wind loads, high stiffness of of the lead plug attracts most of the load and the arrangement shows high stiffness. Under extreme seismic loads lead is deformed plastically and hence the stiffness of the device drops to just the stiffness of rubber. In addition, during the plastic deformation of the lead plug, energy is being dissipated in a hysteretic manner. During extreme events the lead plug experiences the same deformation as rubber but generates heat or dissipates kinetic energy by converting it into heat. Thus, hysteretic behavior of the plug helps reduce the energy absorbed by the building. Therefore, lead rubber bearings show desirable hysteretic damping characteristics, which enhances the structural response of the system. The amount of dissipated energy is a function of maximum bearing displacement. Lead rubber bearings are also easy to install, manufacture, analyze and design [Naeim and Kelly, 1999].

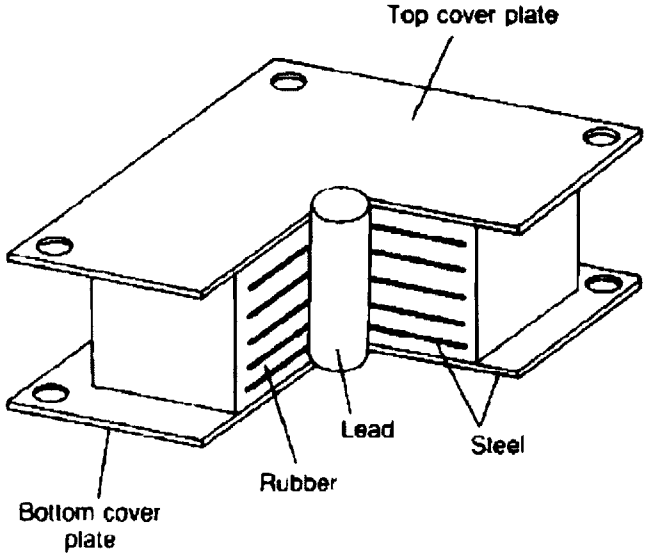

Figure 2.2 – Lead rubber bearing schematic [Kunde and Jangid, 2003]

2.1.3 High Damping Natural Rubber Bearings

The use of high damping natural rubber bearings eliminates the need for supplementary damping devices. Their composition is similar to that of the natural rubber bearings except for the type of elastometric material used. The increase in damping is achieved through the addition of fillers such as carbon, oils and resins. The addition of fillers increased the damping to 20-30% of critical damping.

At shear strains below 20% the high damping natural rubber bearings exhibit high stiffness and high damping. This behavior is advantageous for limiting deflections under service wind loads. At shear strains between 20 and 120% their shear modulus (and hence stiffness) remains constant and damping decreases. At strains above 120% there is an increase in damping and stiffness. Therefore, such behavior provides sufficient stiffness for service wind loads and also limits deflections and effectively dissipates energy during under extreme earthquake loads. High damping natural rubber bearings share the advantages with the aforementioned devices with regard to ease of manufacture and implementation [Naeim and Kelly, 1999].

2.2 Sliding Devices

The primary advantage of sliding devices is their ability to eliminate torsional effects in asymmetric structures. This is because the frictional force utilized in sliding devices is proportional to the axial force on a sliding device due to weight. Therefore, the center of gravity of a building coincides with the center of stiffness of the isolation system thus eliminating torsional effects in asymmetric structures [Kunde and Jangid, 2003] and [Trombetti et al., 2001]. The prevalent sliding base isolation devices include pure friction devices, resilient friction based devices and friction pendulums. The details of the aforementioned devices will be discussed in this following section. Furthermore, they are characterized by insensitivity to the frequency content of the earthquake excitations and hence can be used for a range of structures.

2.2.1 Pure Friction Bearings

Pure friction bearings are the earliest type of sliding devices. They essentially represent a sliding joint, which decouples superstructure from the ground. Under service wind loads the structure behaves like a fixed base building because the load is not sufficient to overcome the static friction force. Under high seismic loads static friction is overcome and the bearing slides. Energy is dissipated in the bearings through friction in the

form of Coulomb damping. The lateral force required to overcome static friction is a function of the friction coefficient and the axial force on a bearing due to weight of the superstructure. Friction coefficient can be controlled by selecting appropriate materials for the sliding surfaces of bearings. Significant disadvantages include regular maintenance to ensure friction coefficient is consistent as the bearing ages; and inability of the structure to re-center itself after an earthquake (resilience) [Kunde and Jangid, 2003].

2.2.2 Cable Friction Bearings

The schematic layout of cable friction bearings is shown in Figure 2.3. The device consists of a conventional sliding bearing , high strength restrainer cables and if necessary, a shear bolt in the middle.Under extreme earthquake events restrainer cables restrict excessive displacement of the superstructure. Under minor and moderate earthquakes, the shear bolt is designed not to break so that no replacement of the bearing will be necessary. Under high earthquake loads the shear bolt breaks, and sliding is mobilized. Thus the transmission of earthquake forces to the superstructure is mitigated. Energy is dissipated through friction between stainless steel plate and the teflon plate while excessive relative displacements are restricted by cables [Wancheng et al., 2012].

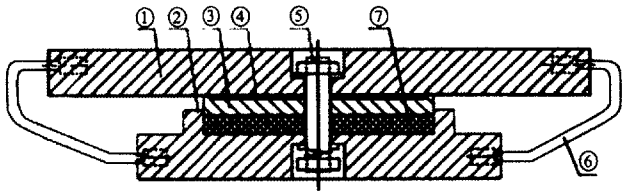

(1) upper plate (2) lower plate (3) stainless steel plate (4) teflon plate (5) shear bolt (6) cable (7) elastomeric pad

Figure 2.3 – Cable friction bearing schematic [Wancheng et al., 2012]

2.2.3 Resilient Friction Base Isolators

As shown in Figure 2.4, the resilient friction-base isolators are composed of a set of flat metal plates which can slide on each other with a central rubber core and/or peripheral rubber cores. The rings are enclosed in a very flexible rubber cover, which protects the metal rings from corrosion and dust. To reduce the friction, the sliding plates are coated with teflon. The rubber cores help to distribute the lateral displacement and velocity along the height of the isolator. The resilient friction-base isolators is characterized

by the coefficient of friction of the sliding elements and the total lateral stiffness of the rubber cores. The friction developed between the plates is adequate to provide resistance against service wind loads. Under seismic loads, the damping capability of the rubber is small, and the friction damping is the main energy dissipator. As the rubber cores are only fitted but not bonded to the sliding rings, the manufacture of a resilient friction-base isolator is a relatively simple task [Mostaghel and Khodaverdian, 1987].

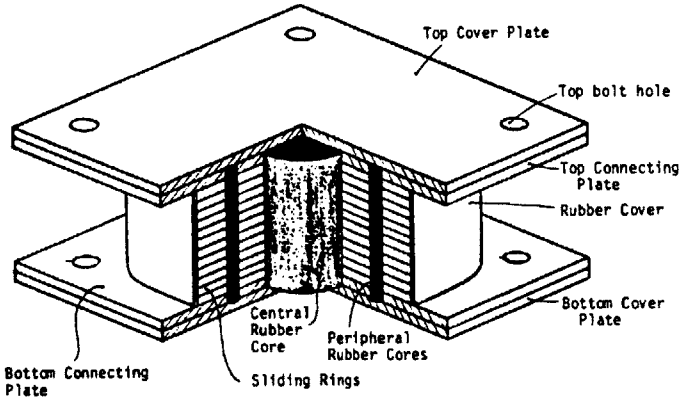

Figure 2.4 – Cable friction bearing schematic [Mostaghel and Khodaverdian, 1987]

2.2.4 Friction Pendulum Bearings

Friction pendulum bearings combine sliding with pendulum action. The schematic layout of a friction pendulum bearing is shown in Figure 2.5. They consist of an articulated slider on a spherical concave chrome surface. The slider is covered with a polished bearing material such as teflon. The friction coefficient between the surfaces is of the order of 0.1 at high velocity sliding and of the order of 0.05 at low velocities. Just as with the conventional sliding bearings, friction pendulum systems act as a fuse and is activated when earthquake forces exceed the value of static friction. Lateral force developed by such bearings is a combination of frictional force and the restoring force due to the rising of the building up the spherical surface. The restoring force in a bearing is proportional to the weight supported by the bearing and inversely proportional to the radius of curvature of the concave surface. Due to static friction, such bearings do not deflect (exhibit rigidity) under service wind loads, which is a highly desirable characteristic. Furthermore, the lateral force in a particular bearing is proportional to the fraction of building weight supported by that bearing and therefore the center of mass of the building is coincident with the center of stiffness of the support system, which eliminates torsional effects. This characteristic has been confirmed by

Zayas et al. [1987] in shake-table tests. In addition, friction pendulum systems show low sensitivity to the frequency content of earthquake excitation and high stability [Mokha et al., 1991].

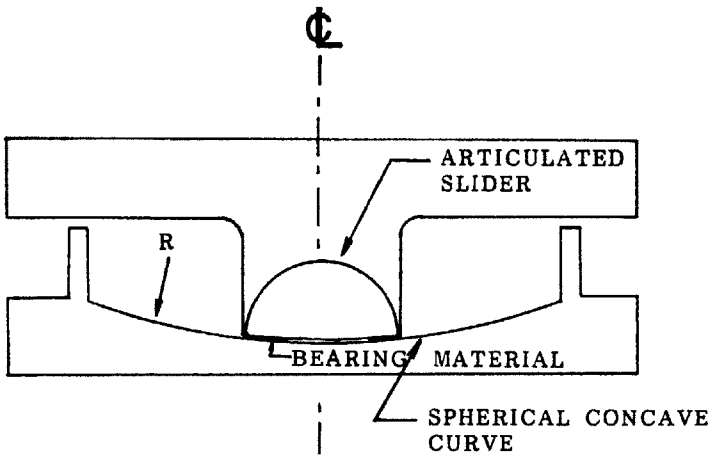

Figure 2.5 – Friction pendulum bearing schematic [Tsai, 1997]

2.3 Limiting Devices

In case of an extreme seismic event, limiting devises may be required to control the displacement of the structure. This is particularly important in case of elastometric bearing systems as they may become unstable at high lateral strains. Excessive lateral deflections may cause collusions with adjacent buildings, which is likely to lead to severe injuries and even loss of life.

Rigid or deformable devices can be used to limit excessive deflections of the bearing systems. However, If during an earthquake a building hits a limiting device, structural accelerations may increase and local damage to the building or the support system may occur due to impact. Thus, designing an appropriate limiting arrangement is an important part of the base isolation design process.

Chapter 3

Methodology

3.1 General Overview

In this study the performance of a six story braced moment steel frame structure subjected to severe earthquake loads was evaluated using elastic/linear analyses. Based on the findings from the analysis, a base isolation system was designed for the structure. The parameters of base isolation system were chosen using the theory of multi degree of freedom dynamic systems. Then base isolation parameters were included into the initial model and the performance of the isolated structure subjected to the same seismic loads was evaluated. The two sets of results were compared and the structural effectiveness of base isolation system for that particular building was discussed. In addition, economic and practical aspects of base isolation systems were discussed and the conclusion with regard to feasibility of the system was drawn based on both structural and economic arguments.

The general methodology adopted for this study was as follows:

- A theoretical discretized lumped mass model of a five story building was calibrated for stiffness to obtain the natural period of oscillation of 1 second using eigenvalue analysis. The detailed process is described in Chapter 4
- Based on the results from the discretized model analysis, lateral bracing system for the building was designed
- A model of a six story steel braced moment frame was made using the structural analysis software SAP2000. Detailed description of the building model is given in section 3.2. For this study, the code design methods of IBC-06/09 and AISC according to LRFD were used [International Code Council, 2006].

- Modal analysis of the building was performed and the actual fundamental period of the structure was compared to the period of 1 second, for which the building was designed.
- Static response spectrum analysis of the structure was performed in accordance with the code methods of IBC-06/09.
- Dynamic time-history analysis of the structure was performed. The structure was subjected to the 1940 El Centro earthquake (also known as the 1940 Imperial Valley earthquake). The strong-motion records from both earthquakes were made available by the Pacific Earthquake Engineering Research Center [UCBerkeley, 2010].
- Base isolation parameters were chosen and the bearings were designed.
- Same response spectrum and time-history analyses were performed but on an isolated building.
- Based on the results feasibility of base isolation system was discussed both from structural and economic point of view.

In what follows, is the detailed description of the aforementioned points.

3.2 Building Description

The building is an six-story Steel Moment Resisting Frame with diagonal cross bracing. It is square in plan, with dimensions 67.5×67.5 ft. Story height is 15 ft and therefore the total height of the building is 90 feet. The lateral resistance in both orthogonal directions comprises of a three-bay moment resisting frame with tension cross braces across the central bay as shown in Figures 3.1 and 3.2. Spacing between columns is 22.5 ft in both directions. All the column sections are W14×82 and all the beam sections are W16×45. The floor system is the same at all floors and comprises of beams at 11.25 ft spacing in one direction and 22.5 ft spacing in the other with an 8 inch concrete slab. Figure 3.3 shows the floor framing arrangement. All columns are oriented in the same direction with their stronger bending axis in the X-Z plane. The structural steel used is Grade A992 of 50 ksi yield strength.

In addition to the self weight of the framing, the gravity loads on the structure comprise of the uniformly distributed dead load of 100 psf imposed on the slabs due to its self weight and a live load of 75 psf on each floor except the roof. The roof has a dead load of 100 psf due to slab self weight and a live load of 20 psf.

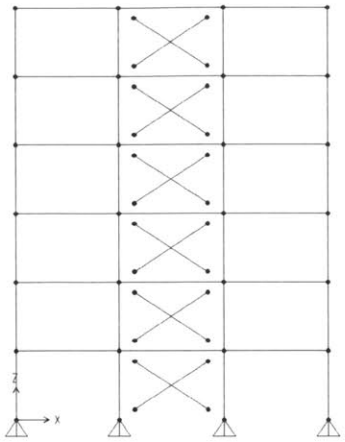

Figure 3.1 – Building frame elevation view

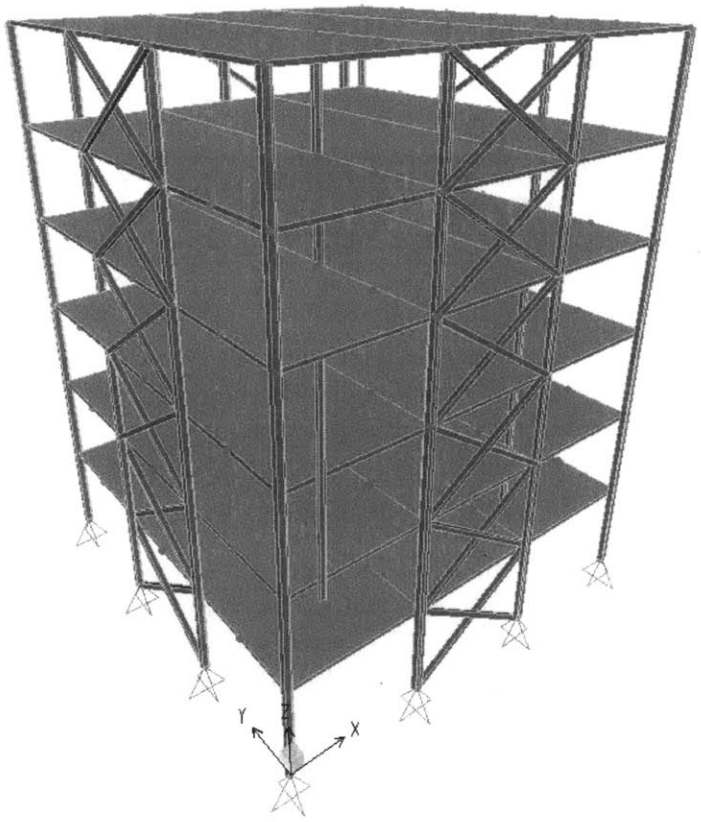

Figure 3.2 – Building frame 3-d view

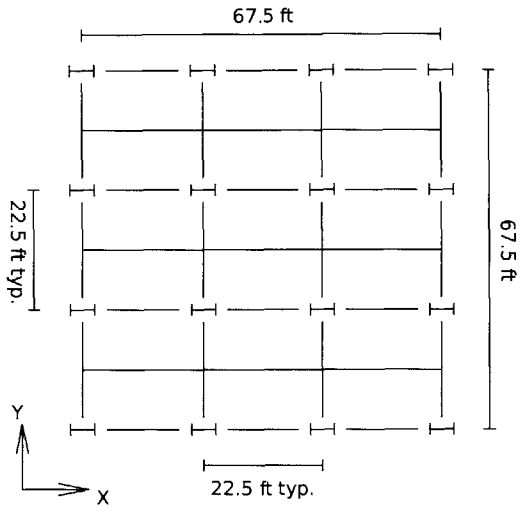

Figure 3.3 – Floor framing plan

3.3 Modeling the Structure: Nuances, Assumptions, Directions

The nuances of modeling the structure and performing analyses are described in detail in this section.

The primary lateral resisting system for all the building consists of a moment resisting frame and a cross bracing. Columns and beams were modeled as *frame* elements while the floor slabs were modeled as *thin shell* elements. To ensure that the bracing acts in pure axial action, *moment releases* were assigned at the ends of bracing members. Elsewhere, no moment releases were assigned. The columns of the structure was assumed to be moment connected at the base. Therefore, a *fixed joint restraint* was assigned at the nodes corresponding to the base connections of the structure.

In order to ensure that, in the model, the beams do not act as composite members with the floor slab i.e. the floor slab does not act in compression as a top flange of the beams, area stiffness properties of the shell elements were modified. This command can be found by first selecting the shell elements, then by going into *Assign - Area Stiffness Modifiers* and setting the *Membrane f11 Modifier* and *Membrane f22 Modifier* to zero. This command prohibits in-plane axial loads in two orthogonal directions to be taken by the slabs. The command ensures that the shell area elements do not take any compression and hence do not induce composite beam behavior by acting as additional compressive top flanges of beams.

Although prohibiting in-plane axial forces in the shell elements allows to accurately model beam behavior in bending, it also means that any lateral loads are taken entirely by floor framing elements and nodes in any particular floor are free to move relative to one another. In reality, the slab will restrain any relative movements between the nodes and the floors' behavior will be closer to that of a rigid body. To prohibit the relative movement between the nodes at each story, they were assigned a diaphragm constraint. Each floor needs to be assigned a separate diaphragm constraint, otherwise the relative motion of the nodes between stories will be inhibited and the whole building will behave as a rigid body. This command can be accessed by selecting the relevant nodes at each story, then clicking on *Assign - Joint - Constraints* and choosing Diaphragm as a constraint type and setting an axis normal to the plane of the floor slab (i.e. Z-axis) as a constraint direction. This command ensures rigid body behavior of the floors.

The mass and gravity loads from the framing however were included in the analytical model. Each member was assigned gravity loads. The gravity loads consisted of the self-weight of the member and any supported dead load that corresponded to the weight of the structure distributed to that member. A dead load of 100 psf was imposed on top of the shell elements representing the self weight of an 8 inch-thick concrete floor slab (specific weight of concrete,γ_c=150 pcf). In addition to the dead load, a live load of 75 psf was imposed in top of the slabs to represent.

To accurately simulate the dynamic behavior, the *Mass Source* for the model was defined to be taken from *Element and Additional Masses and Loads*. This command can made by selecting the *Define - Mass Source* and clicking on *Element and Additional Masses and Loads* in the *Mass Definition* section. For the dead load a multiplier of 1 was selected. For the live load a multiplier 0.75 was selected to imitate the building being not fully occupied during an earthquake event. [Computers and Structures, 2012]

Chapter 4

Stiffness Calibration and Base Isolation Design

This section describes the process of stiffness calibration for the building so that its period was around 1 second. The structure shown in Figure 3.1 is modeled as a multi degree of freedom beam shown in Figure 4.1. According to Connor [2002]: *"For actual buildings, the ratio of height to width (i.e., aspect ratio) provides an indication of the relative contribution of shear versus bending deformation. Buildings with aspect ratios on the order of unity tend to display shear beam behavior ... On the other hand, buildings with aspect ratios greater than about 7 display bending beam behavior..."* In case of the building in this study, the aspect ratio is given by:

$$\frac{H}{B} = \frac{90ft}{67.5ft} = 1.33 \tag{4.1}$$

The aspect ratio is of the order of 1, therefore shear deformation dominates in the building, hence discretized shear beam model is suitable for calculations.

This section will present the detailed calculations for calibrating stiffness using the matrix method. The MATLAB code was written to perform the computations, which can be found in Appendix A. In order to facilitate the reader's understanding, both numerical and algebraic expressions will be developed in this chapter.

4.1 Building Stiffness Calibration

4.1.1 Discretized Five Degree of Freedom Model

Masses m_1 to m_5 for the discrete model shown in Figure4.1 are calculated based on floor loads and weight of structural members. The results are summarized in Table 4.1.

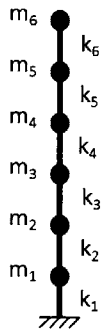

Figure 4.1 – Discretized lumped mass model

Floor	1	2	3	4	5	6
Weight of columns (*kips*)	9.84	19.68	19.68	19.68	19.68	9.84
Weight of beams (*kips*)	33.41	33.41	33.41	33.41	33.41	33.41
Weight of slab (*kips*)	455.63	455.63	455.63	455.63	455.63	455.63
Weight due to live loads (*kips*)	441.72	441.72	441.72	441.72	441.72	91.13
Total weight of floor (*kips*)	940.6	950.4	950.4	950.4	950.4	590.0
m_i $(kips\frac{s^2}{in})$	2.43	2.46	2.46	2.46	2.46	1.53

Table 4.1 – Nodal mass distribution for a discretized model

Note that in order to convert kilo-pound force units into imperial mass units, the values need to be divided by a factor g=386.4 $\frac{in}{s^2}$

4.1.2 Matrix Method for Stiffness Calibration

The fundamental mode vector, Φ is specified such that the relative nodal displacements for the five elements are equal. This mode vector produces a linear displacement profile

for the fundamental mode. It is defined as:

$$\mathbf{\Phi} = \frac{1}{6}\begin{bmatrix}1\\2\\3\\4\\5\\6\end{bmatrix} \tag{4.2}$$

The mass matrix is given by:

$$\mathbf{M} = \begin{bmatrix} m_1 & 0 & 0 & 0 & 0 & 0 \\ 0 & m_2 & 0 & 0 & 0 & 0 \\ 0 & 0 & m_3 & 0 & 0 & 0 \\ 0 & 0 & 0 & m_4 & 0 & 0 \\ 0 & 0 & 0 & 0 & m_5 & 0 \\ 0 & 0 & 0 & 0 & 0 & m_6 \end{bmatrix} \tag{4.3}$$

The values of $m_1 ... m_6$ are nodal masses given in Table 4.1

The stiffness matrix is given by:

$$\mathbf{K} = \begin{bmatrix} k_1 + k_2 & -k_2 & 0 & 0 & 0 & 0 \\ -k_2 & k_2 + k_3 & -k_3 & 0 & 0 & 0 \\ 0 & -k_3 & k_3 + k_4 & -k4 & 0 & 0 \\ 0 & 0 & -k_4 & k_4 + k_5 & -k_5 & 0 \\ 0 & 0 & 0 & -k_5 & k_5 + k_6 & -k_6 \\ 0 & 0 & 0 & 0 & -k_6 & k_6 \end{bmatrix} \tag{4.4}$$

In order to find lateral stiffness coefficients for each story ($k_1 ... k_6$), the equation 4.5 is applied:

$$\omega^2 \mathbf{M\Phi} = \mathbf{K\Phi} \tag{4.5}$$

We want to calibrate the stiffness in such a way that the fundamental period of the building was 1 second. Therefore:

$$\omega = \frac{2\pi}{T} = \frac{2\pi}{1s} = 6.28\frac{rad}{s} \tag{4.6}$$

Conducting matrix multiplication of equation 4.5 we obtain a matrix expression characterized by a set of six linear equations:

$$\begin{bmatrix} 6.580m_1 \\ 13.159m_2 \\ 19.739m_3 \\ 26.318m_4 \\ 32.898m_5 \\ 39.478m_6 \end{bmatrix} = \frac{1}{6} \begin{bmatrix} k_1 - k_2 \\ k_2 - k_3 \\ k_3 - k_4 \\ k_4 - k_5 \\ k_5 - k_6 \\ k_6 \end{bmatrix} \tag{4.7}$$

Substituting the values from Table4.1 into equation 4.7 we obtain the following numerical values:

$$\begin{bmatrix} 15.99 \\ 32.37 \\ 48.56 \\ 64.74 \\ 80.93 \\ 60.40 \end{bmatrix} = \frac{1}{6} \begin{bmatrix} k_1 - k_2 \\ k_2 - k_3 \\ k_3 - k_4 \\ k_4 - k_5 \\ k_5 - k_6 \\ k_6 \end{bmatrix} \tag{4.8}$$

Finally, using back-substitution we obtain lateral stiffness coefficients for all stories:

$$\begin{bmatrix} k_1 \\ k_2 \\ k_3 \\ k_4 \\ k_5 \\ k_6 \end{bmatrix} = \begin{bmatrix} 1818 \\ 1722 \\ 1528 \\ 1237 \\ 848 \\ 362 \end{bmatrix} \frac{kips}{in} \tag{4.9}$$

Using this result, it is now possible to design a bracing system for the building. This process is described in the following section.

4.1.3 Contribution of Columns to Stiffness

The structure is a moment frame and therefore the columns contribute significantly to the building's lateral stiffness. Before selecting sections for lateral bracing, the contribution of the columns needs to be deducted from the lateral stiffness coefficients. According to Connor [2002], the column shear stiffness coefficients can be approximated

by assuming that the inflection points in the columns and beams are at their midpoints such as shown in Figure 4.2.

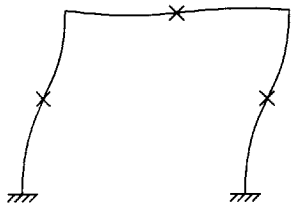

Figure 4.2 – Assumed deformed shape of columns and beams (crosses mark the inflection points)

Based on the aforementioned assumption, the lateral stiffness of columns is given by the following expression:

$$k_{internal} = \frac{12EI_{column}}{h^3(1+r)} \tag{4.10}$$

and

$$k_{external} = \frac{12EI_{column}}{h^3(1+2r)} \tag{4.11}$$

where h is the story height and r is defined by:

$$r = \frac{I_{column}L_{beam}}{I_{beam}h} \tag{4.12}$$

The fundamental mode of structures has to be in the least stiff direction of the structure. Because the bending stiffness of W-sections about the minor axis is much smaller that about the major axis, the fundamental mode will be in the same direction as the minor bending axis of columns. Therefore, the second moment of area value for the columns is taken about the minor axis. With the readily available values for the second moments of area, the contribution of columns to lateral stiffness can be readily computed using equations 4.10, 4.11 and 4.12.

$$r = \frac{I_{column}L_{beam}}{I_{beam}h} = \frac{148in^4 \times 270in}{586in^4 \times 180in} = \frac{111}{293} = 0.379 \tag{4.13}$$

$$k_{external} = \frac{12EI_{column}}{h^3(1+2r)} = \frac{12 \times 29000ksi \times 148in^4}{(180in)^3(1+2\times 0.379)} = 5.02\frac{kips}{in} \tag{4.14}$$

$$k_{internal} = \frac{12EI_{column}}{h^3(1+r)} = \frac{12 \times 29000ksi \times 148in^4}{(180in)^3(1+0.379)} = 6.40\frac{kips}{in} \tag{4.15}$$

Knowing that each story has 8 external columns and 8 internal columns, the total lateral stiffness contribution from columns per story is:

$$k_{columns} = 8(k_{internal} + k_{external}) = 8 \times (5.02 + 6.40)\frac{kips}{in} = 91.4\frac{kips}{in} \tag{4.16}$$

Now, the contribution of columns to lateral stiffness is known and the required total lateral stiffness coefficients have also been obtained as described in Section 4.1.2. With these quantities bracing can be designed so that the building had the desired period of 1 second. For each story, shear stiffness from bracing equals the required total shear stiffness (as found in Section 4.1.2) less the stiffness contribution from columns.

$$k_i^{brace} = k_i - k_{columns} \tag{4.17}$$

where i=1...6 is the story number. Table 4.2 presents summary of the stiffness coefficients required from the bracing on each story.

Story	k_i	$k_{columns}$	k_{brace}
1	1818	91.4	1727
2	1722	91.4	1631
3	1528	91.4	1437
4	1237	91.4	1146
5	848	91.4	757
6	362	91.4	271

Table 4.2 – Summary of lateral stiffness parameters (all units are $\frac{kips}{in}$)

It is of interest to visualize the distribution of the required brace stiffness on each floor. The plot showing this distribution is presented in Figure 4.3.

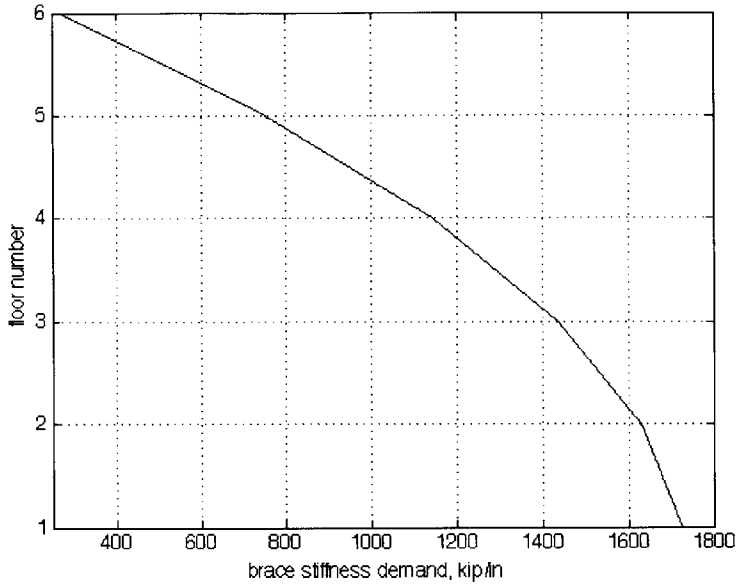

Figure 4.3 – Distribution of brace stiffness by floor

4.1.4 Selecting Brace Sizes

Having determined the required lateral stiffness coefficients for the bracing, we can select the appropriate bracing sizes using the available section sizes in the AISC manual and equations 4.18, 4.19, 4.20 and 4.21, where h, b and θ are shown in Figure 4.4. The selected secions for braces on each story are summarized in Table 4.3.

$$k_i^{brace} = \frac{AE}{L} cos\theta \tag{4.18}$$

$$cos\theta = \frac{b}{\sqrt{h^2 + b^2}} \tag{4.19}$$

$$L = \sqrt{h^2 + b^2} \tag{4.20}$$

$$A = \frac{k(h^2 + b^2)}{Eb} \tag{4.21}$$

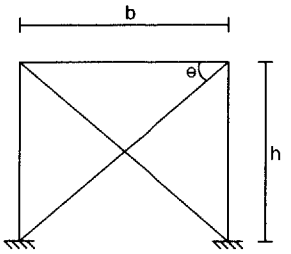

Figure 4.4 – Bay dimensions

Story	$k_i^{brace}(\frac{kips}{in})$	$A_{required}(in^2)$	Section	$A_{provided}(in^2)$	$\Delta A(in^2)$
1	1727	23.23	HSS14×14×1/2	24.60	1.37
2	1631	21.93	HSS16×0.500	22.70	0.77
3	1437	19.33	HSS16×0.438	19.90	0.57
4	1146	15.41	HSS12×12×3/8	16.00	0.59
5	757	10.18	HSS8×8×3/8	10.40	0.22
6	271	3.64	HSS3.5×3.5×4/8	4.09	0.45

Table 4.3 – Summary of lateral stiffness parameters

Because the braces were chosen from the list of available section sizes given in the AISC manual, the actual provided cross sectional brace areas are slightly different from the required ones. Therefore the shear stiffness of each story is slightly different from what is required. The actual stiffness coefficients for each story are summarized in Table 4.4.

Story	$k_{actual}^{brace}, (\frac{kips}{in})$	$k_{col's}, (\frac{kips}{in})$	$k_i^{actual}, (\frac{kips}{in})$	$k_i, (\frac{kips}{in})$	$\Delta k_i(\%)$
1	1829	91.4	1921	1818	5.6
2	1688	91.4	1779	1722	3.3
3	1480	91.4	1571	1528	2.8
4	1190	91.4	1281	1237	3.6
5	773	91.4	865	848	2.0
6	304	91.4	396	362	9.3

Table 4.4 – Actual stiffness coefficients for each story

4.2 Base Isolation Design

Having determined the natural period and the response of the fixed-base structure to earthquake loads, one can start selecting parameters for the base isolation system. Let us suppose that we want to reduce accelerations experienced by the structure from 1.5g to about 0.4g. From the plot in Figure 5.3 the equivalent period of the structure needs to be shifted from 1s to about 3s to 4s. In fact, at T=3.5s the acceleration value equals 0.4114g So we chose the natural equivalent period of the isolated structure, T_{eq}=3.5s.

In what follows, is the described procedure for selecting base isolator stiffness parameters and designing base isolation devices.

4.2.1 Isolator Stiffness Calibration

For selecting base isolation stiffness parameters, the procedure described by Connor [2002] was adopted. Initially, periods need to be converted to angular frequencies. The actual value of natural period of the fixed-base structure found by conducting modal analysis in SAP2000, T=1.09 seconds, which is very close to the value for which bracing system was designed. For the purpose of preliminary isolation sizing the fixed base natural period of 1 second was selected.

$$\omega_{eq} = \frac{2\pi}{T_{eq}} = \frac{2\pi}{3.5} = 1.795\frac{rad}{s} \tag{4.22}$$

$$\omega_n = \frac{2\pi}{T_n} = \frac{2\pi}{1s} = 6.283\frac{rad}{s} \tag{4.23}$$

Where $\tilde{k}$ is the equivalent modal frequency and $\tilde{m}$ is the equivalent modal mass. They are given by the following expressions:

$$\tilde{m} = \mathbf{\Phi}^T \mathbf{M} \mathbf{\Phi} \tag{4.24}$$

$$\tilde{m} = \frac{1}{36}\begin{bmatrix}1 & 2 & 3 & 4 & 5 & 6\end{bmatrix}\begin{bmatrix} m_1 & 0 & 0 & 0 & 0 & 0 \\ 0 & m_2 & 0 & 0 & 0 & 0 \\ 0 & 0 & m_3 & 0 & 0 & 0 \\ 0 & 0 & 0 & m_4 & 0 & 0 \\ 0 & 0 & 0 & 0 & m_5 & 0 \\ 0 & 0 & 0 & 0 & 0 & m_6 \end{bmatrix}\begin{bmatrix}1\\2\\3\\4\\5\\6\end{bmatrix} \tag{4.25}$$

$$\tilde{m} = \frac{1}{36}(m_1 + 4m_2 + 9m_3 + 16m_4 + 25m_5 + m_6) \tag{4.26}$$

Plugging in the values of m_1 to m_6 previously found in section 4.1.1 and summarized in Table 4.1 we obtain:

$$\tilde{m} = 5.2875 kips\frac{s^2}{in} \tag{4.27}$$

$$\tilde{k} = \mathbf{\Phi}^T \mathbf{K} \mathbf{\Phi} \tag{4.28}$$

The values of k_i^{actual} were calculated and summarized in Table 4.4. Plugging them into the general stiffness matrix formulation gives:

$$\mathbf{K} = \begin{bmatrix} 3700 & -1779 & 0 & 0 & 0 & 0 \\ -1779 & 3350 & -1571 & 0 & 0 & 0 \\ 0 & -1571 & 2852 & -1281 & 0 & 0 \\ 0 & 0 & -1281 & 2146 & -865 & 0 \\ 0 & 0 & 0 & -865 & 1261 & -396 \\ 0 & 0 & 0 & 0 & -396 & 396 \end{bmatrix} \frac{kips}{in} \tag{4.29}$$

$$\tilde{k} = \mathbf{\Phi}^T \mathbf{K} \mathbf{\Phi} = 217\frac{kips}{in} \tag{4.30}$$

Having established the numerical values for the modal mass and stiffness, $\tilde{m}$ and $\tilde{k}$, we can select the appropriate stiffness coefficient for the bearings so that the equivalent period of the isolated structure was 3.5 seconds.

$$\omega_{eq} = \Gamma \omega_n \tag{4.31}$$

$$\Gamma = \frac{\omega_{eq}}{\omega_n} = \frac{2}{7} = 0.286 \tag{4.32}$$

$$\Gamma = \frac{k_b}{\tilde{k} + k_b} \tag{4.33}$$

Therefore,

$$k_b = \frac{\Gamma \tilde{k}}{1 - \Gamma} = \frac{2\tilde{k}}{5} = 86.8\frac{kips}{in} \tag{4.34}$$

The calculated value of bearing stiffness can now be used to design the actual bearing devices.

4.2.2 Bearing Design

Due to the numerous advantages friction pendulum isolation systems described in Chapter 2, they were chosen for this study. The stiffness of an individual bearing is given by:

$$k_b = \frac{W_b}{R} \tag{4.35}$$

where W_b is the weight taken by an individual bearing and R is the radius of curvature of the bearing. The weight taken by each bearing is equal to axial load in the columns. As was mentioned before, the gravity loads on the structure were set to be dead load plus 75% of live load. The result of the static analysis in SAP2000 has shown the axial load of 446.4 kips. Knowing this value, the radius of curvature of the friction pendulum can be designed. Also, k_b is the total stiffness of the whole bearing system. There are 16 columns in the building. Each column needs to have a bearing underneath it. The bearings under the building act like springs in parallel. Therefore the stiffness of an individual bearing, $k_{b,ind}$ needs to be:

$$k_{b,ind} = \frac{k_b}{16} = \frac{86.8}{16}\frac{kips}{in} = 5.425\frac{kips}{in} \tag{4.36}$$

$$R = \frac{W_b}{k_b} = \frac{446.4kips}{5.425\frac{kips}{in}} = 82.3in = 6ft10in \tag{4.37}$$

Having obtained the required parameters for the lateral system and base isolation, we can proceed to conducting simulations and analyses to investigate how the fixed base structure and the isolated structure respond to earthquake excitation.

Chapter 5

Analyses

In order to successfully design the base isolating system for the structure the dynamic response of the unisolated structure needs to be studied. A series of analyses involving fixed-base structure was performed on the building using SAP2000 nonlinear finite software. The primary objective of the analyses is to study the displacements, inter-story drifts and stresses in the structure under earthquake loads. The fundamental period found through modal analysis was compared to the target period of 1 second and reasons for discrepancy were discussed. The target period of 1 second was chosen to put the structure at the top plateau of the response spectrum curve, so that seismic forces experienced by the structure were at their maximum. This was done in order to demonstrate how effectively base isolation reduces earthquake effects.

5.1 Fixed-Base Structure

5.1.1 Modal Analysis

In order to find the period of the structure, linear modal analysis was performed. Because the analysis is linear, it is possible to design tension-only bracing by using only one diagonal member working both in tension and compression. In the linear range, it produces the same effect as the tension-only cross bracing. It is possible to model tension-only bracing by assigning compression limits to frame members, but such method only works in non-linear analysis cases and hence is not suitable for linear modal case.

The modal periods of the building for the first three global modes are given in Table 5.1.

Mode 1, had a fundamental period of 1.09 seconds in the y direction and mode 2 had a period of 1.04 in the x direction. The first torsional mode had a period of 0.67 seconds. Notably, modal analysis has shown that the difference between the actual fundamental period and the desired period of 1 second for which the stiffness was calibrated is 0.09 seconds or 9%, which is high level of accuracy.

The images showing mode shapes magnified 150 times are displayed in Figures 5.1 and 5.2.

T_1, (s)	T_2, (s)	T_3, (s)
1.09	1.04	0.67

Table 5.1 – Global modal periods: Fixed Base Structure

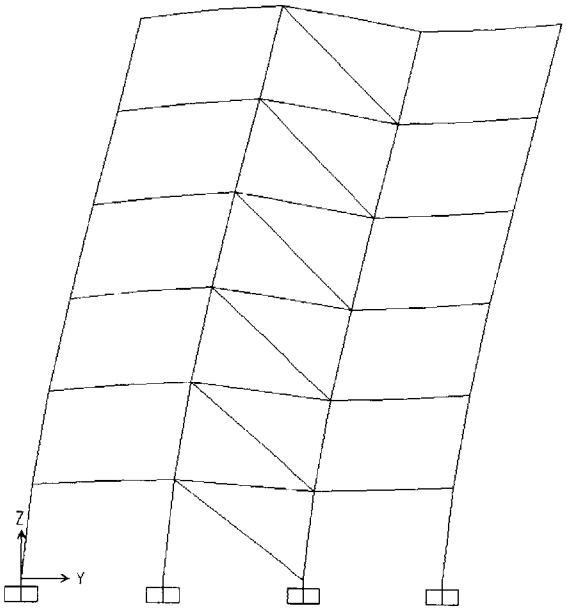

Figure 5.1 – First mode shape (T_1=1.09s)

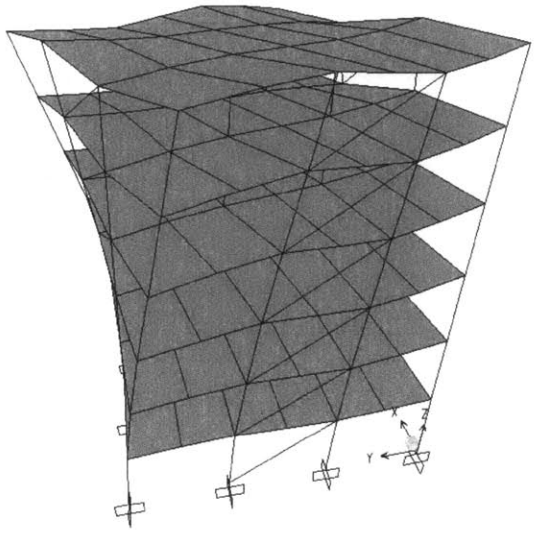

Figure 5.2 – Torsional mode shape (T_3=0.67s)

The first two mode shapes are very similar in shape except they are in two orthogonal directions. Therefore, an image of the second mode shape was omitted. The main finding of modal analysis is that the building actually has the fundamental period, which is very close to the one for which the lateral stiffness system was designed.

5.1.2 Response Spectrum Analysis

The response spectrum curve was constructed in accordance with the IBC-06/09 code.The site parameters were deliberately chosen so that the conditions were unfavorable and earthquake induced accelerations were increased. The value of S_1 was chosen as 2.5g, and S_s was given a value of 0.9g. As it is known that soft clay soils amplify earthquake accelerations. The work by Krawinkler and Rahnama [1992] supports this point. Therefore, the site soil type was chosen as soft clay. Soft clay corresponds to site class E. Long period transition period, T_n was set to 12 s. Using these parameters the response spectrum curve is plotted as shown in Figure 5.3. The period of natural oscillation of our building, T=1s places the structure right at the top plateau of the response spectrum curve, with accelerations of 1.5g.

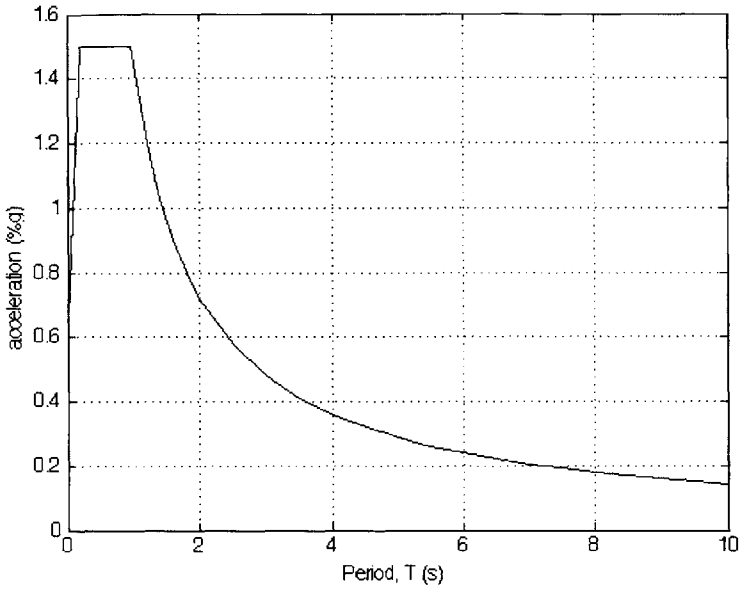

Figure 5.3 – Response spectrum curve

The result of response spectrum analysis has shown the lateral displacement at the top of the structure of u_{top}=1.73ft, which gives a drift of γ=0.019. The building does not pass the maximum drift requirement even with a lax drift limit of 1/250=0.004. Therefore, the results of response spectrum analysis suggest that, in order for the building to be safe additional measures for providing earthquake resistance are required.

5.1.3 Time History Analysis

The earthquake ground motions used in this study are the actual ground motions recorded at the base of the building during the 1940 El Centro Earthquake. These motions include components in the x (North-South) and y (East-West) directions shown. The acceleration time history in the z direction was not included in the analysis as the study by John A. Martin Associates [1999] showed that the effects of vertical excitation were insignificant. The acceleration time history of the earthquake in the North-South direction is presented in Figure 5.4. The focus is on the North-South component of accelerations as they are the stronger motions and hence the North-Sound component controls the design process. The building response is presented as a displacement time history of the top story and is shown in Figure 5.5.

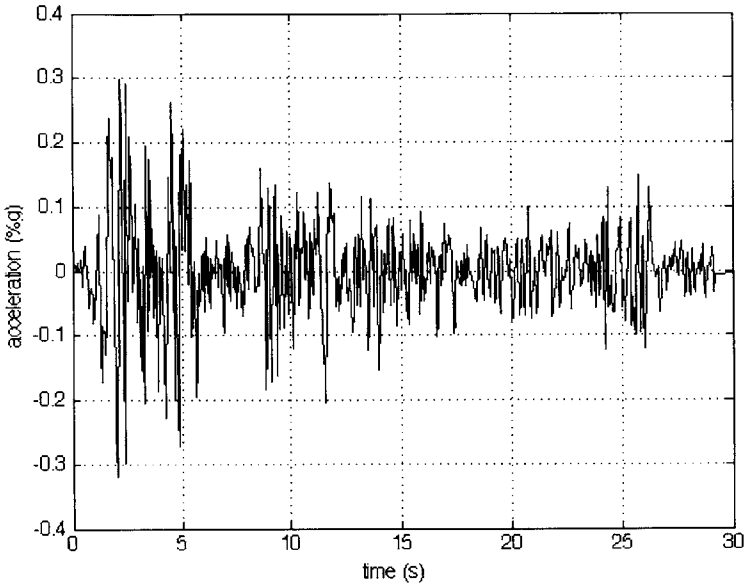

Figure 5.4 – El Centro Earthquake May 18, 1940, North-South component

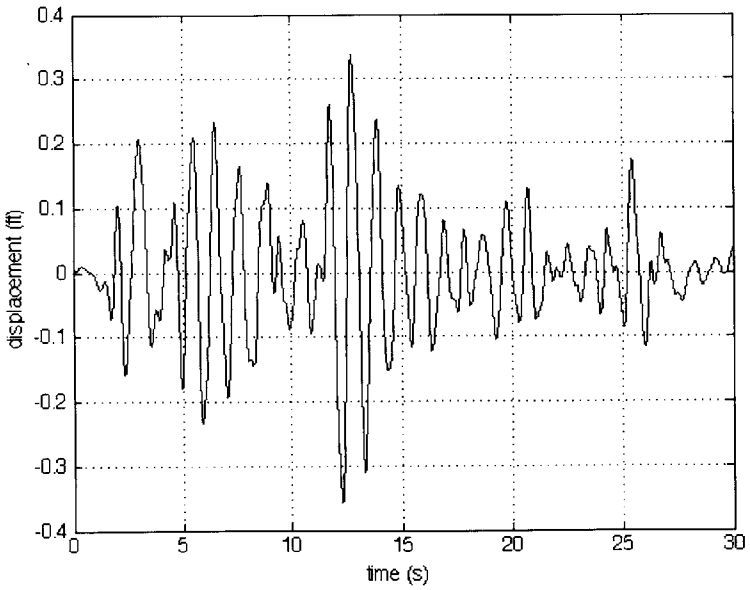

Figure 5.5 – Top story displacement

As can be seen from Figure 5.5. the maximum displacement at the top story was fond to be u_{top}=0.36ft, which gives a drift of γ=0.004. Although the building just satisfies the drift limit of 1/250, the limit itself is lax. Typically, it is recommended to limit the drifts to 1/400 or 1/500. Therefore, the results of time history analysis also suggest that additional measures to provide seismic safety are required for this building.

5.2 Isolated Structure

5.2.1 Modeling Base Isolation

Base isolation was modeled as a roller support, which allows translations in x and y directions but prohibits translations in the z direction. A *Spring* constraint was added to the nodes at the base to simulate the behavior of isolators. All the nodes on the plane where columns meet the ground were assigned a diaphragm constraint normal to the z axis, to imitate the action of a mat, which prohibits the relative motion between the nodes in the x-y plane. In addition all the nodes on the plane of the mat were assigned a body constraint to prohibit the relative motion between the nodes in the z plane.

Every node at the base was assigned a *Spring* constraint with the stiffness coefficient of 5.425 kips/in as found in section 4.2.2. The analysis results are presented in the following sections.

5.2.2 Modal Analysis

In order to find the equivalent period of the base isolated structure, linear modal analysis was performed. Again, because the analysis is linear, it is possible to design tension-only bracing by using only one diagonal member working both in tension and compression.

The modal periods of the building for the first three global modes are given in Table 5.2 . Mode 1, had a fundamental period of 3.62 seconds in the y direction and mode 2 had a period of 3.61 in the x direction. The first torsional mode had a period of 2.97 seconds. The images showing mode shapes magnified 200 times are displayed in Figures 5.6 and 5.7. The first two mode shapes are very similar in shape except they are in two orthogonal directions. Therefore, an image of the second mode shape was omitted. Notably, because the base stiffness is much lower than the structural stiffness, the first three global shapes represent almost rigid body movement of the structure,

and all the displacement happens at the isolated base. This is clearly seen in Figures 5.6 and 5.7.

Most importantly, modal analysis has shown that base isolation has shifted the natural period of the building away from the peak of the response spectrum curve shown in Figure 5.3. The accelerations have reduced from 1.5g to below 0.5g, which is more than a 65% reduction.

T_1, (s)	T_2, (s)	T_3, (s)
3.62	3.61	2.97

Table 5.2 – Global modal periods: isolated structure

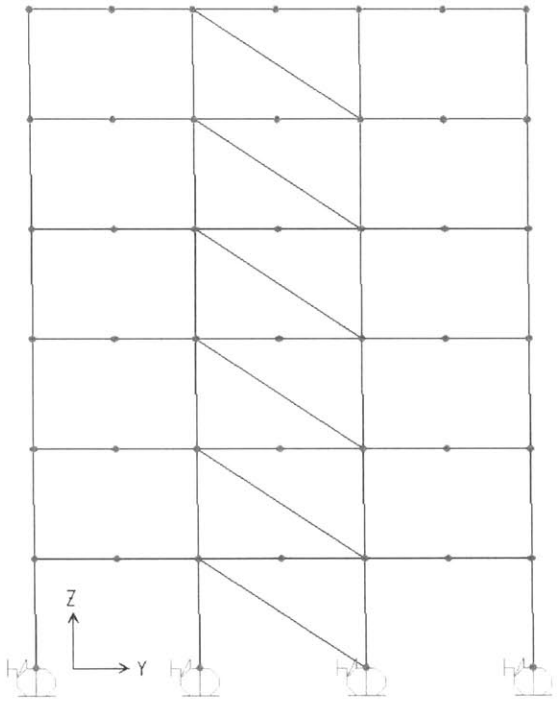

Figure 5.6 – First mode, xy axes show origin position (T_1=3.62s)

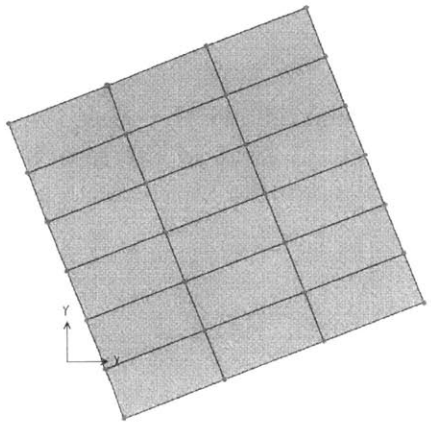

Figure 5.7 – Torsional mode shape, rigid body rotation of the building (T_3=2.97s)

5.2.3 Response Spectrum Analysis

The result of response spectrum analysis has shown the lateral displacement at the base u_{base}=3.6ft, and the top, u_{top}=3.9ft, which gives a total drift of γ=0.0033=1/300. Adding base isolation has filtered the input earthquake excitation i.e. moved the building down the response spectrum curve. The inertia forces taken by the structure have reduced substantially and hence the drift was reduced. Thus, the result suggests that adding base isolation substatially helped increase the building's earthquake resistance.

5.2.4 Time History Analysis

The acceleration time history of the earthquake in the North-South direction is presented in Figure 5.4. The displacement response at the base of the building is shown in Figure 5.8. As can be seen, the maximum displacement of the base with respect to the ground is 0.73 ft. The displacement response at the top of the building is shown in Figure 5.9. By comparing graphs Figures in 5.8 and 5.9, one can note that they are almost the same. This suggests that there is very little relative displacement between the top story and the base. The relative displacement response at the top of the building with respect to the base is in Figure 5.10. The maximum displacement of the roof with respect to the ground is 0.83ft. Hence the lateral displacement of the building with respect to the base is 0.1 ft, which gives a very small shear ratio of 1/900. Hence, with the addition of base isolation, the building totally capable of withstanding earthquake loads comparable to El Centro. Thus, time history analysis has shown that base isolation has substantially improved the building's seismic performance.

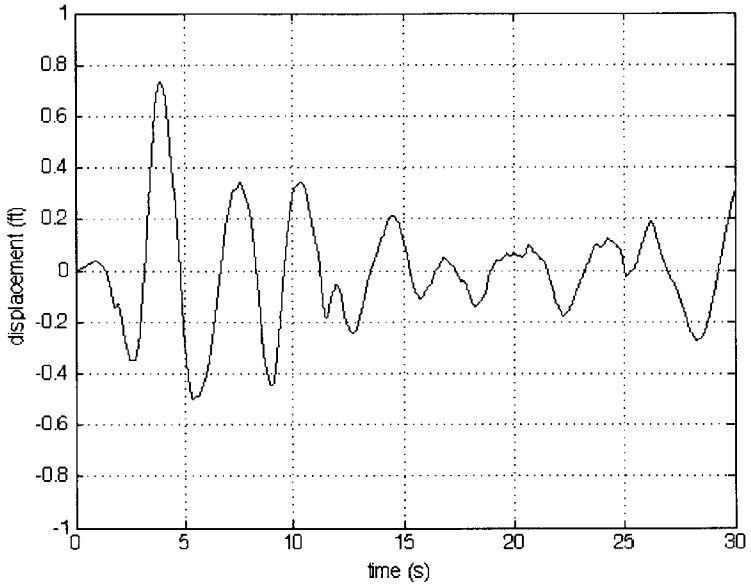

Figure 5.8 – Displacement response at the base of the building

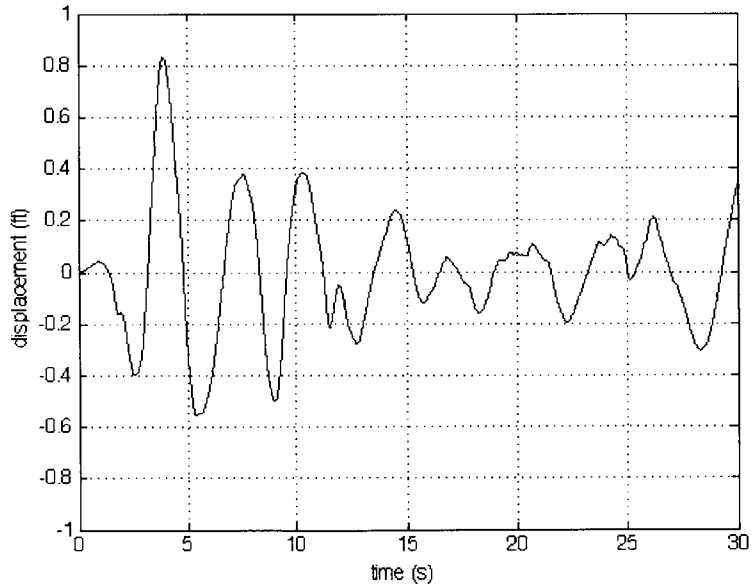

Figure 5.9 – Displacement response at the top of the building

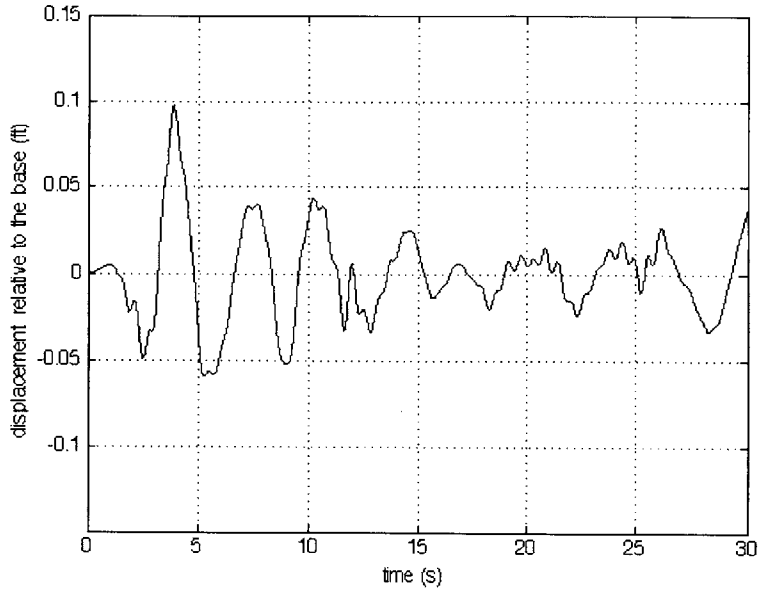

Figure 5.10 – Relative displacement response of the roof with respect to the base

5.2.5 Summary

The isolated period and the elastic base stiffness characterize a base isolated structure. The period of the structure has increased from a fixed-base value of 1.09 seconds to 3.62 seconds for the fundamental mode. According to the results of response spectrum analyses of both buildings, such period shift reduces accelerations by over 65%.The two similar graphs shown in Figures 5.8 and 5.9 indicate how little a difference there is between the base and top story displacement. By comparing results from section 5.1.3 with the results from section 5.2.4, in particular, Figure 5.5 and Figure 5.10, one can observe that the maximum displacement has reduced from 0.36 ft to 0.1 ft, which is almost a four-fold reduction.

Thus, having conducted a series of analyses with a fixed-base and isolated structures, we can conclude that base isolation is an effective measure for substantially improving earthquake resistance of buildings.

Chapter 6

Conclusion

The series of analyses has proven the benefits of base isolation. The stiffness parameters of bearings were designed and analyzed to maximize the seismic performance of the structure. Base isolation has displayed significant positive effects by increasing the structure's natural period and hence reducing inertia forces on the structure. This investigation outlined the major relevant issues concerning the conceptual design of a base isolated structure. The parameters of the building and the site conditions chosen for the study were deliberately chosen in such a way that the earthquake effects were most severe. In reality, the stiffness calibration approach can be integrated together with the base isolation design in early stages of projects in order to develop structures of high seismic performance.

Bibliography

Andriono, T. (1990, May). *Seismic Resistant Design of Base Isolated Multistorrey Structures.* Ph. D. thesis, University of Canterbury. 12

Charng, P.-H. (1998, December). *Base Isolation for Multistorey Building Structures.* Ph. D. thesis, University of Canterbury. 13

Computers and Structures (2012). *SAP2000 Integrated Finite Element Analysis and Design of Structures, Analysis Reference.* Berkeley, California, USA: Computers and Structures. 29

Connor, J. (2002). *Introduction to Structural Motion Control.* Massachusetts Institute of Technology. 12, 31, 34, 39

Ehrlich, E., S. B. Flexner, G. Carruth, and J. Hawkins (1980). *Oxford American Dictionary.* Avon Books. 18

International Code Council (2006). *Interational Building Code.* International Code Council. 25

Jenkins, H. *Velocity Displacement for NS El Centro Acceleration.* Mercer University.

Krawinkler, H. and M. Rahnama (1992). Effects of soft soils on design spectra. In A. Balkema (Ed.), *Proceedings of the Tenth World Conference on Earthquake Engineering*, Volume 10, pp. 5841–5844. 45

Kunde, M. and R. Jangid (2003). Seismic behavior of isolated bridges: A state-of-the-art review. *Electronic Journal of Strucutral Engineering 3*, 140–170. 9, 18, 19, 20, 21

Mokha, A., M. Constantinou, A. Reinhorn, and V. Zayas (1991). Experimental study of friction-pendulum isolation system. *Journal of Structural Engineering 117*(4), 1201–1217. 23

Mostaghel, N. and M. Khodaverdian (1987). Dynamics of resilient-friction base isolator. *Earthquake Engineering and Structural Dynamics 15*, 379–390. 9, 22

Naeim, F. and J. Kelly (1999). *Design of Isolated Structures from Theory to Practice.* John Wiley Sons. 19, 20

Skinner, R. and G. McVerry (1975). Base isolation for increased earthquake resistance of buildings. *Bulletin of New Zealand Society for Earthquake Engineering 8*(2), 93–101. 12, 13

Trombetti, T., C. Ceccoli, and L. Silvestri (2001). A simplified approach to the analysis of torsional problems in seismic base isolated structures. In A. Singh (Ed.), *Creative Systems in Structural and Construction Engineering.* 20

Tsai, C. (1997). Finite element formulations for friction pendulum seismic isolation bearings. *International Journal for Numerical Methods in Engineering 40*(29-49). 9, 23

UCBerkeley (2010). Peer ground motion database. Technical report, Pacific Earthquake Engineering Research Center:. 26

Wancheng, Y., W. Binbin, C. Pakchiu, C. Xinjian, and R. Zhaojun (2012). Seismic performance of cable-sliding friction bearing system for isolated bridges. *Eathquake Engineering and Engineering Vibration 11*(2), 173–183. 9, 21

Zayas, V., S. Low, and S. Mahin (1987). The fps earthquake resisting system, experimental report. Technical Report UCB/EERC-87/01,, Earthquake Engineering Research Center, University of California, Berkeley. 23

Appendix A

MATLAB code used for matrix stiffness calibration method

```
format short

syms k1 k2 k3 k4 k5 k6 m1 m2 m3 m4 m5 m6

M=[2.43 0 0 0 0 0;
      0 2.46 0 0 0 0;
      0 0 2.46 0 0 0;
      0 0 0 2.46 0 0;
      0 0 0 0 2.46 0;
      0 0 0 0 0 1.53]

M1=[m1 0 0 0 0 0;
        0 m2 0 0 0 0;
        0 0 m3 0 0 0;
        0 0 0 m4 0 0;
        0 0 0 0 m5 0;
        0 0 0 0 0 m6]

omega=2*pi

phi=(1/6)*[1;2;3;4;5;6]
```

```
K=[k1+k2 -k2 0 0 0 0;
    -k2 k2+k3 -k3 0 0 0;
    0 -k3 k3+k4 -k4 0 0;
    0 0 -k4 k4+k5 -k5 0;
    0 0 0 -k5 k5+k6 -k6;
    0 0 0 0 -k6 k6]

omegamfi=omega^2*M*phi

Kphi=K*phi

k6=6*omegamfi(6)
k5=6*omegamfi(5)+k6
k4=6*omegamfi(4)+k5
k3=6*omegamfi(3)+k4
k2=6*omegamfi(2)+k3
k1=6*omegamfi(1)+k2

omegaM1phi=omega^2*M1*phi
vpa(omegaM1phi)

phit=phi';
phitM1phi=phit*M1*phi
phitMphi=phit*M*phi

Kvals=[k1+k2 -k2 0 0 0 0;
           -k2 k2+k3 -k3 0 0 0;
           0 -k3 k3+k4 -k4 0 0;
           0 0 -k4 k4+k5 -k5 0;
           0 0 0 -k5 k5+k6 -k6;
           0 0 0 0 -k6 k6]

phitKvalsphi=phit*Kvals*phi
ka1=1921;
ka2=1779;
ka3=1571;
ka4=1281;
ka5=865;
ka6=396;
```

```
KA=[ka1+ka2 -ka2 0 0 0 0;
       -ka2 ka2+ka3 -ka3 0 0 0;
       0 -ka3 ka3+ka4 -ka4 0 0;
       0 0 -ka4 ka4+ka5 -ka5 0;
       0 0 0 -ka5 ka5+ka6 -ka6;
       0 0 0 0 -ka6 ka6]

phitKAsphi=phit*KA*phi
```

RESULTS

```
M =

    2.4300         0         0         0         0         0
         0    2.4600         0         0         0         0
         0         0    2.4600         0         0         0
         0         0         0    2.4600         0         0
         0         0         0         0    2.4600         0
         0         0         0         0         0    1.5300


M1 =

[ m1,  0,  0,  0,  0,  0]
[  0, m2,  0,  0,  0,  0]
[  0,  0, m3,  0,  0,  0]
[  0,  0,  0, m4,  0,  0]
[  0,  0,  0,  0, m5,  0]
[  0,  0,  0,  0,  0, m6]


omega =

    6.2832


phi =

    0.1667
    0.3333
    0.5000
    0.6667
    0.8333
    1.0000
```

```
K =

[ k1 + k2,     -k2,        0,        0,        0,   0]
[     -k2, k2 + k3,     -k3,        0,        0,   0]
[       0,     -k3, k3 + k4,     -k4,        0,   0]
[       0,       0,     -k4, k4 + k5,     -k5,   0]
[       0,       0,       0,     -k5, k5 + k6, -k6]
[       0,       0,       0,       0,     -k6,  k6]


omegamfi =

   15.9888
   32.3723
   48.5585
   64.7446
   80.9308
   60.4020


Kphi =

 k1/6 - k2/6
 k2/6 - k3/6
 k3/6 - k4/6
 k4/6 - k5/6
 k5/6 - k6/6
        k6/6
```

```
k6 =

  362.4119


k5 =

  847.9964


k4 =

   1.2365e+03


k3 =

   1.5278e+03


k2 =

   1.7220e+03


k1 =

   1.8180e+03
```

```
omegaM1phi =

  (2778046668940015*m1)/422212465065984
  (2778046668940015*m2)/211106232532992
  (2778046668940015*m3)/140737488355328
  (2778046668940015*m4)/105553116266496
 (13890233344700075*m5)/422212465065984
   (2778046668940015*m6)/70368744177664


ans =

  6.579736267392905328203293417 27*m1
 13.159472534785810656406586834 54*m2
 19.739208802178715984609880251 81*m3
 26.318945069571621312813173669 08*m4
 32.898681336964526641016467086 35*m5
 39.478417604357431969219760503 62*m6



phitM1phi =

m1/36 + m2/9 + m3/4 + (4*m4)/9 + (25*m5)/36 + m6


phitMphi =

    5.2875
```

```
Kvals =

   1.0e+03 *

    3.5400   -1.7220         0         0         0         0
   -1.7220    3.2499   -1.5278         0         0         0
         0   -1.5278    2.7643   -1.2365         0         0
         0         0   -1.2365    2.0845   -0.8480         0
         0         0         0   -0.8480    1.2104   -0.3624
         0         0         0         0   -0.3624    0.3624


phitKvalsphi =

  208.7421


KA =

        3700        -1779            0            0            0            0
       -1779         3350        -1571            0            0            0
           0        -1571         2852        -1281            0            0
           0            0        -1281         2146         -865            0
           0            0            0         -865         1261         -396
           0            0            0            0         -396          396


phitKAsphi =

  217.0278
```

```
stiffness_calibration

M =

    2.4300         0         0         0         0         0
         0    2.4600         0         0         0         0
         0         0    2.4600         0         0         0
         0         0         0    2.4600         0         0
         0         0         0         0    2.4600         0
         0         0         0         0         0    1.5300


M1 =

[ m1,  0,  0,  0,  0,  0]
[  0, m2,  0,  0,  0,  0]
[  0,  0, m3,  0,  0,  0]
[  0,  0,  0, m4,  0,  0]
[  0,  0,  0,  0, m5,  0]
[  0,  0,  0,  0,  0, m6]


omega =

    6.2832


phi =

    0.1667
    0.3333
    0.5000
    0.6667
    0.8333
    1.0000
```

```
K =

[ k1 + k2,     -k2,        0,        0,        0,   0]
[     -k2, k2 + k3,     -k3,        0,        0,   0]
[       0,     -k3, k3 + k4,     -k4,        0,   0]
[       0,       0,     -k4, k4 + k5,     -k5,   0]
[       0,       0,       0,     -k5, k5 + k6, -k6]
[       0,       0,       0,       0,     -k6,  k6]



omegamfi =

   15.9888
   32.3723
   48.5585
   64.7446
   80.9308
   60.4020



Kphi =

 k1/6 - k2/6
 k2/6 - k3/6
 k3/6 - k4/6
 k4/6 - k5/6
 k5/6 - k6/6
        k6/6
```

```
k6 =

  362.4119

k5 =

  847.9964

k4 =

   1.2365e+03

k3 =

   1.5278e+03

k2 =

   1.7220e+03

k1 =

   1.8180e+03
```

```
omegaM1phi =

  (2778046668940015*m1)/422212465065984
  (2778046668940015*m2)/211106232532992
  (2778046668940015*m3)/140737488355328
  (2778046668940015*m4)/105553116266496
 (13890233344700075*m5)/422212465065984
   (2778046668940015*m6)/70368744177664


ans =

  6.579736267392905328203293417 27*m1
 13.159472534785810656406586834 54*m2
 19.739208802178715984609880251 81*m3
 26.318945069571621312813173669 08*m4
 32.898681336964526641016467086 35*m5
 39.478417604357431969219760503 62*m6


phitM1phi =

m1/36 + m2/9 + m3/4 + (4*m4)/9 + (25*m5)/36 + m6


phitMphi =

    5.2875
```

```
Kvals =

   1.0e+03 *

    3.5400   -1.7220         0         0         0         0
   -1.7220    3.2499   -1.5278         0         0         0
         0   -1.5278    2.7643   -1.2365         0         0
         0         0   -1.2365    2.0845   -0.8480         0
         0         0         0   -0.8480    1.2104   -0.3624
         0         0         0         0   -0.3624    0.3624


phitKvalsphi =

  208.7421


KA =

        3700       -1779           0           0           0           0
       -1779        3350       -1571           0           0           0
           0       -1571        2852       -1281           0           0
           0           0       -1281        2146        -865           0
           0           0           0        -865        1261        -396
           0           0           0           0        -396         396


phitKAsphi =

  217.0278
```

Appendix B

MATLAB code for processing earthquake data

```
%  earthquake-NS.m
%
%  Code which inputs, plots ground acceleration and ground velocity of the
% 1940 El Centro earthquake. North-South acceleration data.


%  Load the data
load elcentro_NS.txt -ascii
%  Column 1 time ; Column 2 acceleration G's
data = elcentro_NS;
accn = data(:,2);
t = data(:,1);
dt=t(2)-t(1);
%  Create the times that go with the acceleration.
```

```
%  Plot the time-accn data
subplot(2,1,1)
plot(t,accn,'black'); set(gca,'FontSize',13)
grid
title('N-S Acceleration History 1940 El Centro EarthQuake')
xlabel('time (s) ')
ylabel('acceleration (%g)')
axis([0 30 -0.4 0.4])


% Plot the ground velocity
vel(1)=0
for n=1:(length(accn)-1)
    vel(n+1)=vel(n)+ 9.81*accn(n)*dt;
end



subplot(2,1,2)
plot(t,vel,'black'); set(gca,'FontSize',13)
grid
title('N-S Velocity History 1940 El Centro EarthQuake')
xlabel('time (s) ')
ylabel('velocity (m/s)')
```

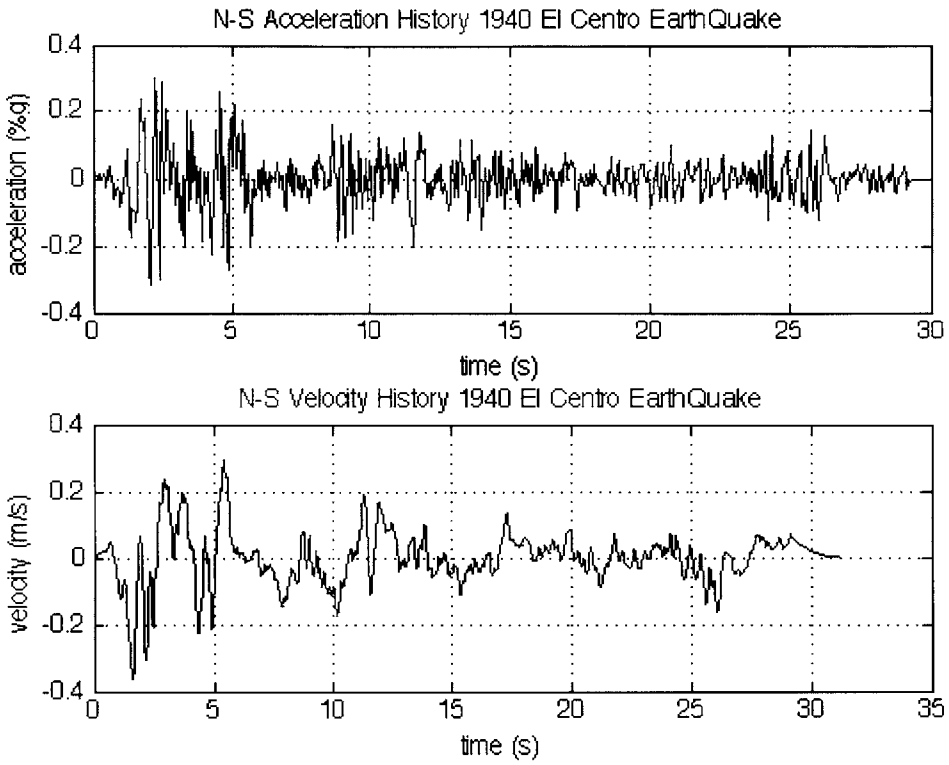

Figure B.1 – Processed earthquake record data